Surface plasmon modes in graphene wedge and groove waveguides

Penghong Liu,[1,2] **Xinzheng Zhang,**[1,2] **Zenghong Ma,**[1,2] **Wei Cai,**[1,2,*] **Lei Wang,**[1,2] **and Jingjun Xu**[1,2,3]

[1]*The Key Laboratory of Weak-Light Nonlinear Photonics, Ministry of Education, School of Physics and TEDA Applied Physics Institute, Nankai University, Tianjin 300457, China*
[2]*Synergetic Innovation Center of Chemical Science and Engineering (Tianjin)*
[3]*jjxu@nankai.edu.cn*
**weicai@nankai.edu.cn*

Abstract: Surface plasmon modes at terahertz-infrared waveband in sub-wavelength graphene wedge and groove waveguides are investigated, which can be categorized into perfect electric conductor and perfect magnetic conductor symmetric modes with different propagation characteristics. The electromagnetic near-fields are localized strongly in different regions for these two kinds of modes. Moreover, these modes can be interpreted by the folded graphene ribbon modes. The brim width of the waveguides and the Fermi energy of the graphene strongly influence the dispersion and propagation distances of the plasmon modes, which can be used for tuning the plasmon modes in graphene wedge and groove waveguides efficiently.

© 2013 Optical Society of America

OCIS codes: (240.6680) Surface plasmons; (250.5403) Plasmonics; (230.7370) Waveguides.

References and links

1. A. K. Geim and K. S. Novoselov, "The rise of graphene," Nat. Mater. **6**, 183–191 (2007).
2. E. H. Hwang and S. Das Sarma, "Dielectric function, screening, and plasmons in two-dimensional graphene," Phys. Rev. B **75**, 205418 (2007).
3. M. Jablan, H. Buljan, and M. Soljačić, "Plasmonics in graphene at infrared frequencies," Phys. Rev. B **80**, 245435 (2009).
4. F. H. L. Koppens, D. E. Chang, and F. J. García de Abajo, "Graphene plasmonics: A platform for strong light-matter interactions," Nano Lett. **11**, 3370–3377 (2011).
5. A. Y. Nikitin, F. Guinea, F. J. Garcia-Vidal, and L. Martin-Moreno, "Fields radiated by a nanoemitter in a graphene sheet," Phys. Rev. B **84**, 195446 (2011).
6. A. Y. Nikitin, F. Guinea, F. J. García-Vidal, and L. Martín-Moreno, "Edge and waveguide terahertz surface plasmon modes in graphene microribbons," Phys. Rev. B **84**, 161407(R) (2011).
7. J. Christensen, A. Manjavacas, S. Thongrattanasiri, F. H. L. Koppens, and F. J. García de Abajo, "Graphene plasmon waveguiding and hybridization in individual and paired nanoribbons," ACS Nano **6**, 431–440 (2012).
8. A. Y. Nikitin, F. Guinea, F. J. Garcia-Vidal, and L. Martin-Moreno, "Surface plasmon enhanced absorption and suppressed transmission in periodic arrays of graphene ribbons," Phys. Rev. B **85**, 081405(R) (2012).
9. P. Liu, W. Cai, L. Wang, X. Zhang, and J. Xu, "Tunable terahertz optical antennas based on graphene ring structures," Appl. Phys. Lett. **100**, 153111 (2012).
10. L. Ju, B. Geng, J. Horng, C. Girit, M. Martin, Z. Hao, H. A. Bechtel, X. Liang, A. Zettl, Y. R. Shen, and F. Wang, "Graphene plasmonics for tunable terahertz metamaterials," Nat. Nanotechnol. **6**, 630–634 (2011).
11. Z. Fei, G. O. Andreev, W. Bao, L. M. Zhang, A. S. McLeod, C. Wang, M. K. Stewart, Z. Zhao, G. Dominguez, M. Thiemens, M. M. Fogler, M. J. Tauber, A. H. Castro-Neto, C. N. Lau, F. Keilmann, and D. N. Basov, "Infrared nanoscopy of dirac plasmons at the graphene-SiO_2 interface," Nano Lett. **11**, 4701–4705 (2011).
12. H. Yan, X. Li, B. Chandra, G. Tulevski, Y. Wu, M. Freitag, W. Zhu, P. Avouris, and F. Xia, "Tunable infrared plasmonic devices using graphene/insulator stacks," Nat. Nanotechnol. **7**, 330–334 (2012).
13. V. W. Brar, M. S. Jang, M. Sherrott, J. J. Lopez, and H. A. Atwater, "Highly confined tunable mid-infrared plasmonics in graphene nanoresonators," Nano Lett. **13**, 2541–2547 (2013).

#200090 - $15.00 USD Received 25 Oct 2013; revised 29 Nov 2013; accepted 9 Dec 2013; published 20 Dec 2013

14. Z. Fang, S. Thongrattanasiri, A. Schlather, Z. Liu, L. Ma, Y. Wang, P. M. Ajayan, P. Nordlander, N. J. Halas, and F. J. Garca de Abajo, "Gated tunability and hybridization of localized plasmons in nanostructured graphene," ACS Nano **7**, 2388–2395 (2013).
15. J. Chen, M. Badioli, P. Alonso-Gonzalez, S. Thongrattanasiri, F. Huth, J. Osmond, M. Spasenovic, A. Centeno, A. Pesquera, P. Godignon, A. Zurutuza Elorza, N. Camara, F. J. G. de Abajo, R. Hillenbrand, and F. H. L. Koppens, "Optical nano-imaging of gate-tunable graphene plasmons," Nature **487**, 77–81 (2012).
16. Z. Fei, A. S. Rodin, G. O. Andreev, W. Bao, A. S. McLeod, M. Wagner, L. M. Zhang, Z. Zhao, M. Thiemens, G. Dominguez, M. M. Fogler, A. H. C. Neto, C. N. Lau, F. Keilmann, and D. N. Basov, "Gate-tuning of graphene plasmons revealed by infrared nano-imaging," Nature **487**, 82–85 (2012).
17. J. Takahara, S. Yamagishi, H. Taki, A. Morimoto, and T. Kobayashi, "Guiding of a one-dimensional optical beam with nanometer diameter," Opt. Lett. **22**, 475–477 (1997).
18. P. Berini, "Plasmon polariton modes guided by a metal film of finite width," Opt. Lett. **24**, 1011–1013 (1999).
19. A. Manjavacas and F. J. García de Abajo, "Robust plasmon waveguides in strongly interacting nanowire arrays," Nano Lett. **9**, 1285–1289 (2009).
20. R. F. Oulton, V. J. Sorger, D. A. Genov, D. F. P. Pile, and X. Zhang, "A hybrid plasmonic waveguide for subwavelength confinement and long-range propagation," Nat. Photonics **2**, 496–500 (2008).
21. I. V. Novikov and A. A. Maradudin, "Channel polaritons," Phys. Rev. B **66**, 035403 (2002).
22. S. I. Bozhevolnyi, V. S. Volkov, E. Devaux, and T. W. Ebbesen, "Channel plasmon-polariton guiding by subwavelength metal grooves," Phys. Rev. Lett. **95**, 046802 (2005).
23. S. I. Bozhevolnyi, V. S. Volkov, E. Devaux, J.-Y. Laluet, and T. W. Ebbesen, "Channel plasmon subwavelength waveguide components including interferometers and ring resonators," Nature **440**, 508–511 (2006).
24. J. Dintinger and O. J. F. Martin, "Channel and wedge plasmon modes of metallic v-grooves with finite metal thickness," Opt. Express **17**, 2364–2374 (2009).
25. D. F. P. Pile, T. Ogawa, D. K. Gramotnev, T. Okamoto, M. Haraguchi, M. Fukui, and S. Matsuo, "Theoretical and experimental investigation of strongly localized plasmons on triangular metal wedges for subwavelength waveguiding," Appl. Phys. Lett. **87**, 061106 (2005).
26. M. Yan and M. Qiu, "Guided plasmon polariton at 2d metal corners," J. Opt. Soc. Am. B **24**, 2333–2342 (2007).
27. E. Moreno, S. Rodrigo, S. Bozhevolnyi, L. Martin-Moreno, and F. Garcia-Vidal, "Guiding and focusing of electromagnetic fields with wedge plasmon polaritons," Phys. Rev. Lett. **100**, 023901 (2008).
28. S. Thongrattanasiri, A. Manjavacas, and F. J. García de Abajo, "Quantum finite-size effects in graphene plasmons," ACS Nano **6**, 1766–1775 (2012).
29. B. Wunsch, T. Stauber, F. Sols, and F. Guinea, "Dynamical polarization of graphene at finite doping," New J. Phys. **8**, 318 (2006).
30. K. S. Novoselov, A. K. Geim, S. V. Morozov, D. Jiang, Y. Zhang, S. V. Dubonos, I. V. Grigorieva, and A. A. Firsov, "Electric field effect in atomically thin carbon films," Science **306**, 666–669 (2004).
31. H. C. Schniepp, K. N. Kudin, J.-L. Li, R. K. Prudłomme, R. Car, D. A. Saville, and I. A. Aksay, "Bending properties of single functionalized graphene sheets probed by atomic force microscopy," ACS Nano **2**, 2577–2584 (2008).
32. L. Wang, W. Cai, X. Zhang, and J. Xu, "Surface plasmons at the interface between graphene and kerr-type nonlinear media," Opt. Lett. **37**, 2730–2732 (2012).

1. Introduction

Graphene, a single layer combined carbon atom sheet, is believed as novel optoelectronic material for applications ranging from the terahertz to the visible spectral region [1]. Recently, graphene is emerging as a 2D plasmonic material [2–5], due to that graphene plasmons can not only confine electromagnetic energy into smaller volume than metallic plasmons, but also be actively controlled by external gating or chemical doping. Surface plasmons in structured doped graphene have been theoretically examined in various structures, including ribbons [6, 7], periodic ribbon arrays [8], disks [4], and rings [9]. Meanwhile, surface plasmons were verified spectroscopically in graphene ribbon arrays [10], graphene sheets [11], graphene/insulator stacks [12], graphene resonators [13], graphene disks and rings [14]. Moreover, the plasmon near-fields in graphene were directly imaged using infrared near-field scattering microscopy [15, 16]. On the other hand, there is still great interest in realization of highly compact optical circuits in nanotechnology. And the design of efficient waveguides with long propagation distance, low bending loss and crosstalk in a wide range of frequencies is very essential. Lots of metallic geometries have been proposed to fulfill this goal [17, 18], for example, closed spaced wires [19] and metallo-dielectric hybrid structures [20]. In addition to this,

#200090 - $15.00 USD Received 25 Oct 2013; revised 29 Nov 2013; accepted 9 Dec 2013; published 20 Dec 2013
(C) 2013 OSA

metallic channel [21–24] and wedge [25–27] plasmon waveguides have been investigated and were believed as efficient propagating plasmon devices. However, these structures were mostly designed for near-infrared to visible applications, whose performance could be only controlled passively by changing geometry parameters, such as the depth [22] or thickness [24] of the wedges and grooves. Whereas in the far-infrared and terahertz ranges, metallic plasmons are not very localized which makes them not suitable for routing applications, thus further studies on efficient waveguides are necessary. So it is natural for us to consider graphene groove and wedge waveguides, because of the intrinsic plasmon effect in graphene.

In this paper, we numerically calculate the plasmon modes in graphene wedge and groove waveguides using the finite element method, and the dispersion and propagation distances of these modes are obtained. Two kinds of plasmon modes exist in both wedge and groove waveguides, which possess perfect electric conductor (PEC) and perfect magnetic conductor (PMC) symmetries, respectively. In these two kinds of plasmon modes, electromagnetic fields are confined in different regions, and show different propagation characteristics. Furthermore, we achieve tuning of plasmon modes by varying the brim width of graphene wedge (groove) waveguides. At last, we discuss how the doping level of graphene affects the propagating plasmons in these waveguides.

2. Calculation methods

The optical response of graphene can be efficiently described by in-plane conductivity, the quantum finite-size effect of graphene can be ignored as the size of graphene structures is larger than 20 nm [28]. The dielectric constant of the graphene is calculated directly by $\varepsilon = 1 + \mathrm{i}\sigma/(\varepsilon_0 \omega d)$, where ε_0 is the permittivity of free space, and d is the thickness of the graphene. The conductivity σ of graphene can be expressed as $\sigma = \sigma_{\text{intra}} + \sigma_{\text{inter}}$, where σ_{intra} and σ_{inter} are the contributions from the intraband and interband transitions of electrons in graphene, respectively. Within random-phase approximation [2, 29], they are given by

$$\begin{aligned}
\sigma_{\text{intra}} &= \frac{2\mathrm{i}e^2 k_B T}{\hbar^2 \pi(\omega + \mathrm{i}/\tau)} \ln[2\cosh(\frac{E_F}{2k_B T})], \\
\sigma_{\text{inter}} &= \frac{e^2}{4\hbar}[\frac{1}{2} + \frac{1}{\pi}\arctan(\frac{\hbar\omega - 2E_F}{2k_B T}) - \frac{\mathrm{i}}{2\pi}\ln\frac{(\hbar\omega + 2E_F)^2}{(\hbar\omega - 2E_F)^2 + (2k_B T)^2}].
\end{aligned}$$

In our calculations, the Fermi energy of the graphene E_F in above equations was set as 0.6 eV unless otherwise stated. The ambient temperature T was 300 K. The τ is the relaxation time of the electrons, which is related to the Fermi velocity $v_f = c/300$ and the electron DC mobility $\mu = 1.0\ \mathrm{m}^2/(\mathrm{Vs})$ [30] through $\tau = \mu E_F / e v_F^2$. The graphene with a thickness of 0.5 nm [4, 7] was assumed lying on a substrate with relative permittivity of 2.

The propagating modes can be written into the form $\mathbf{E}(x,y)\exp(\mathrm{i}\beta k_0 z)$, where $\mathbf{E}(x,y)$ is the transversal electric field distribution, $k_0 = \omega/c$ is the light wave vector in vacuum, and β is the normalized wave vector of the plasmon mode. Then the finite element method is adopted to solve the Maxwell equations to get the eigensolutions of $\mathbf{E}(x,y)$ and β. The real part of β corresponds to the normalized momentum of the waveguide mode, and the imaginary part of β determines the propagation distance L by $L/\lambda_0 = 1/[2\pi \cdot \mathrm{Im}(\beta)]$, where λ_0 is the vacuum light wavelength, L/λ_0 is called the normalized propagation distance.

3. Surface plasmon modes in graphene wedge waveguides

The geometry of the graphene wedge waveguide is shown in Fig. 1(a), where a graphene sheet is laid on the top surface of a wedge structure (substrate). The apex angle of the wedge is θ, and the height h is 50 nm. The top and bottom corners of the wedge are rounded with 2 and 5 nm

#200090 - $15.00 USD Received 25 Oct 2013; revised 29 Nov 2013; accepted 9 Dec 2013; published 20 Dec 2013
(C) 2013 OSA

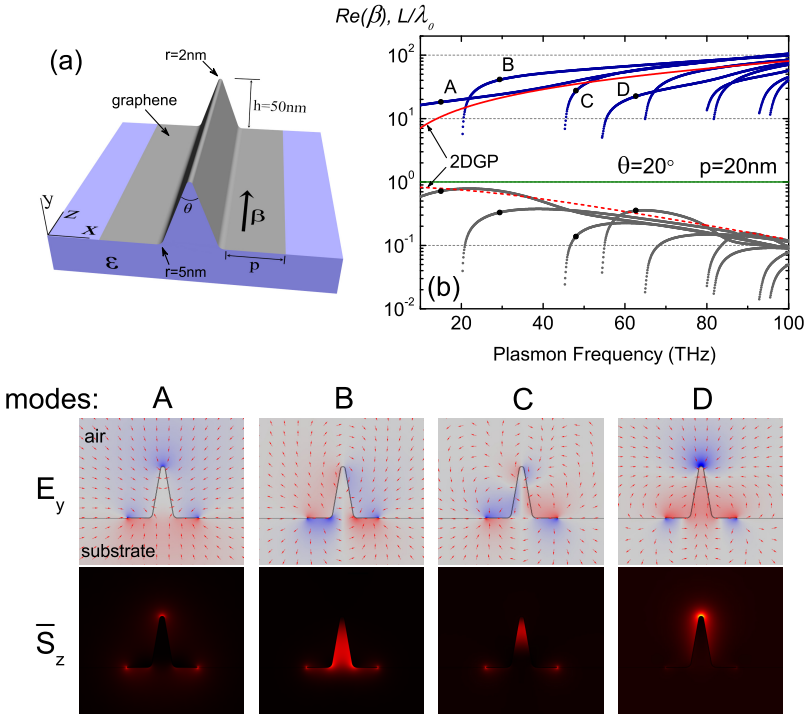

Fig. 1. Plasmon modes in the graphene wedge waveguide. (**a**) The geometry of the wedge waveguide. The plasmons propagate along the z-axis. (**b**) The dispersion of the plasmon modes in the wedge waveguide with $\theta = 20^\circ$ and $p = 20$ nm. Blue lines are the normalized momenta, and gray lines are the normalized propagation distances, the green line in the center corresponds to the momenta of light in vacuum. The lower panels show the E_y and time averaged S_z of the near-fields for the four modes labeled in (**b**). The red arrows represent the flow direction of electric field lines.

curvature radii, respectively. It is experimentally feasible since such sharp graphene structures have been realized by atomic force microscopy [31]. The graphene spreads from the base of the wedge for a distance p, as shown in Fig. 1(a), which is referred as the brim width throughout this paper. The Cartesian coordinate system is shown in the inset, where $x = 0$ corresponds to the plane through the center of the apex, and plasmons propagate along the z axis.

The features of the propagating plasmon modes in the graphene wedge with $\theta = 20^\circ$ and $p = 20$ nm are presented in Fig. 1(b). The normalized momenta and the propagation distances of the plasmon modes are shown with blue and gray lines, respectively. The momentum and propagation distance of the plasmon mode in an extended flat graphene sheet [3], which are termed as 2-D graphene plasmons (2DGPs), are also indicated for comparison (the red solid and dashed lines). As can be seen in Fig. 1(b), it is worth to note that: (i) low-loss propagating plasmon modes stay in the terahertz-infrared range, which can be the indispensable supplement to metallic waveguides; (ii) the maximum energy (100 THz, or 0.41 eV) for the plasmons is smaller than the Fermi energy of graphene (0.6 eV), which indicates that the optical response of graphene mainly comes from intraband transitions of electrons.

To understand the nature of these plasmon modes, the electric near-fields E_y and Poynting vectors $\bar{S}_z$ for the four lower-order modes (labeled as A - D) are shown in Fig. 1 (the lower

#200090 - $15.00 USD Received 25 Oct 2013; revised 29 Nov 2013; accepted 9 Dec 2013; published 20 Dec 2013
(C) 2013 OSA

panels). One can see that the plasmon modes A and D possess perfect electric conductor symmetry (PEC, or $E_x = 0$, $dE_y/dn = 0$, $dH_x/dn = 0$, and $H_y = 0$ along the plane $x = 0$), where the electric fields E_y have reflection symmetry with the plane $x = 0$. The $\bar{S}_z$ of these PEC symmetric modes have similar distribution, where most energy fluxes concentrate above the apex and around the graphene terminations. For the mode D, the electric field lines start from the two terminations of the graphene and end at the apex, indicating that the electrons oscillate vertically along the two inclined sides of the wedge. This is the possible reason for the appearance of the frequency region where the mode D has longer propagation distance than the 2DGP [see $65-80$ THz in Fig. 1(b)]. In contrast, this kind of phenomena does not exist for the plasmon modes of graphene ribbons [5]. On the other hand, the plasmon modes B and C possess the perfect magnetic conductor symmetry (PMC, or $E_y = 0$, $dE_x/dn = 0$, $dH_y/dn = 0$, and $H_x = 0$ along the plane $x = 0$). Unlike the PEC symmetric modes, the energy fluxes in the PMC modes distribute much more in the substrate, and this should be useful if one wants to achieve enhanced light-matter interaction in the substrate, such as enhanced nonlinear effect in the substrate [32].

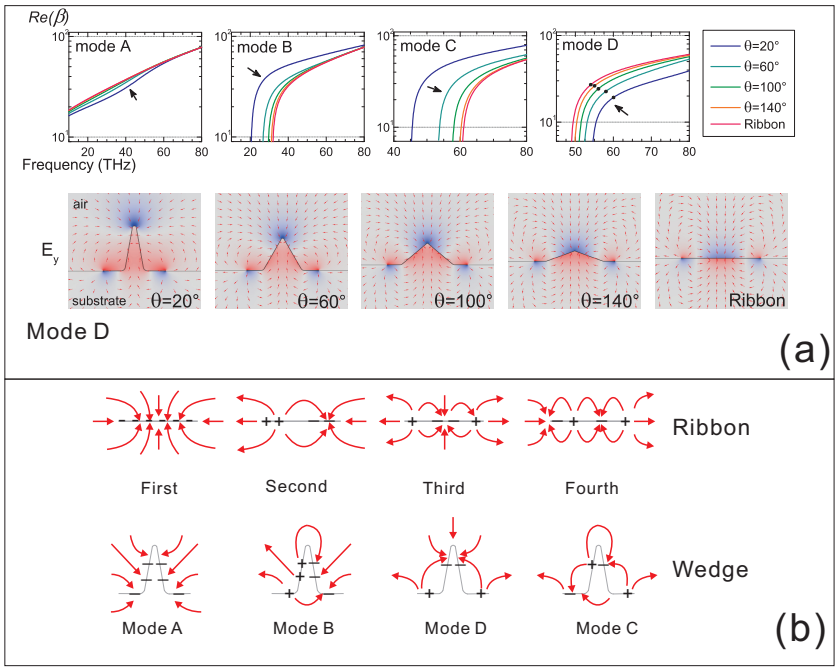

Fig. 2. The evolution of plasmon modes from the graphene wedge to the graphene ribbon. **(a)** The apex angle dependence of the plasmon modes in graphene wedges. The dispersion curves of the modes $A-D$ for the apex angle $20^\circ, 60^\circ, 100^\circ$, and 140° are shown in the top panels, which are compared with the dispersion curves of the corresponding modes in the flat ribbon, respectively. And the lower panels show the near-fields E_y for the points labeled in the dispersion curves of D with different apex angles. **(b)** The charge orderings for the plasmon modes in graphene ribbons and wedges. The PEC symmetric modes in graphene wedges correspond to the odd order modes in ribbons, whereas the PMC symmetric modes correspond to the even order modes.

To further explore the origin of the plasmon modes in the graphene wedge, the evolution of these plasmon modes as the changing of the apex angle is shown in Fig. 2(a). In our calculations, the length of graphene in the transversal section and the brim width are fixed. The

#200090 - $15.00 USD Received 25 Oct 2013; revised 29 Nov 2013; accepted 9 Dec 2013; published 20 Dec 2013
(C) 2013 OSA

plasmon dispersions of modes $A-D$ with the apex angles 20°, 60°, 100°, and 140° are illustrated, compared with the case of the flat graphene ribbon. Taking the mode D for example, the dispersion curves become far away from the dispersion curve of the flat graphene when the apex angle decreases. However, the electric fields E_y always possess three nodes along the transversal section of the graphene. In Fig. 2(b), the charge orderings of plasmon modes for graphene ribbons and wedges are compared. One can find that the PEC and PMC modes in graphene wedges can be simply understood through the graphene ribbon modes by folding the ribbon into the shape of wedge. Specifically, the modes of the graphene ribbon with odd field nodes evolve into PEC modes of the wedge (A and D), whereas the modes with even field nodes become PMC modes (B and C). In contrast to metallic wedges, graphene is a monomolecular layer, it is hard to say that a self-standing graphene is a wedge or a groove. Here whether a structure is identified as a wedge or a groove depends on which side the high permittivity dielectric (substrate) is. Therefor such waveguides can support both PEC and PMC symmetric modes, which is different from the metal wedge waveguides [26].

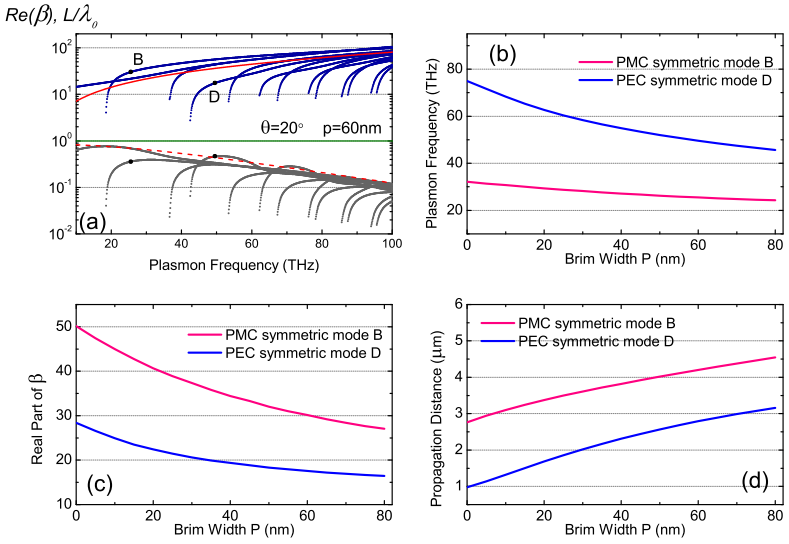

Fig. 3. (**a**) The plasmon modes in the graphene wedge waveguide with an apex angle $\theta = 20^\circ$ and a brim width $p = 60$ nm, the blue and gray lines are the normalized momenta and propagation distances of plasmon modes, respectively. (**b**) - (**d**) The frequencies, momenta, and propagation distances of the PMC symmetric mode B and the PEC symmetric mode D as a function of the brim width.

In the following, we consider using the geometric parameter of wedge structures and the Fermi energy of graphene to tune the propagating plasmon modes. As shown above, the plasmon modes originate from the modes in graphene ribbons. So we first focus on discussing how the brim width p affects the plasmon modes in graphene wedge waveguides. The calculation results for the wedge waveguide with $\theta = 20^\circ$ but a different p value of 60 nm are shown in Fig. 3(a). Compared with Fig.1(b), we get roughly the same dispersion and propagation distance curves, but all the curves are squeezed to the low frequency region, and more modes arise in the frequency range $10-100$ THz, which can be understood by that more higher-order waveguide modes satisfy the resonance condition. Before further discussing how the brim width affects the propagation of plasmons, it is worth to note that there are two different ways to consider tuning

#200090 - $15.00 USD Received 25 Oct 2013; revised 29 Nov 2013; accepted 9 Dec 2013; published 20 Dec 2013
(C) 2013 OSA

the plasmons: (i) to obtain the frequencies where each mode obtains its maximum propagation distance L when the geometry parameters change, because it is more important to know how the geometric parameters affect the whole dispersion curves of the modes; (ii) to care more about how the propagation features of modes change at fixed frequency, which is useful in real-time modulating the propagating plasmon modes in waveguides. Based on this, we calculate the frequencies where the modes B and D obtain their maximum propagation distances L as a function of the brim width p, as shown in Fig. 3(b). Moreover, the normalized momenta and maximum propagation distances L at these frequencies are also shown in Fig. 3(c) and 3(d), respectively. We can see that the frequencies of modes B and D have a blue-shift as the increase of the brim width, accompanying by the decrease of momenta and increase of propagation distances. The reason for choosing mode D rather than mode A is that there is no cutoff frequency for the mode A [see Fig. 1(a)], and the frequency for the maximum propagation distance of the mode A is close to zero.

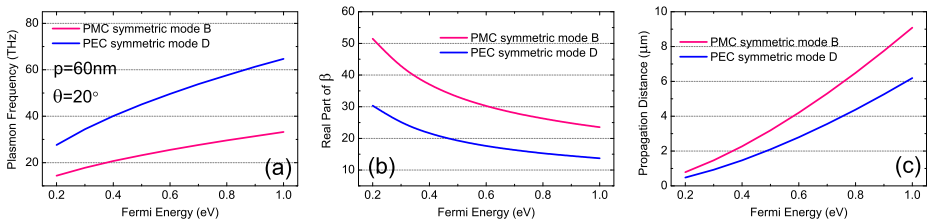

Fig. 4. Doping level dependences of the PMC symmetric mode B and PEC symmetric mode D. (**a**) - (**c**) show the frequencies, momenta, and absolute propagation distances of these two modes as a function of the Fermi energy of graphene.

As we know that plasmons in graphene can also be controlled through adjusting the doping level of the graphene (i.e. the Fermi energy) by electric field gating or chemical doping [4]. In Fig. 4, the doping level dependences of the PMC and PEC symmetric plasmon modes B and D are shown, where the frequencies with maximum propagation distances are chosen again. When the doping level of graphene is raised, the propagation distances of both modes increase with the decrease of the momenta. This is the result of the increase of the carrier density in graphene. Thus raising the Fermi level leads to the similar effects for the propagation distances and momenta as the increase of the brim width. But for the frequencies of the modes, in contrast to increasing the brim width, raising the Fermi energy makes them move to the high frequency region.

For active control of the propagation of the plasmons in real-time, electric field gating can be adopted. In this case, surface plasmons propagating in the waveguide keep a constant frequency. In Fig. 5, we show how the Fermi energy affects the surface plasmons at the fixed frequency 30 THz. The results for the modes A and B are given. The momenta decrease and the propagation distances increase as the increase of the Fermi energy of the graphene. One important fact should be noticed that, since the dispersion curve of the mode B keeps shifting to high frequency as the increase of the Fermi energy [see Fig. 4(a)], the cutoff frequency of the mode B will ultimately get larger than the fixed frequency (30 THz), and the curves in Fig. 5 will also be cutoff. This can happen on each mode except the fundamental mode A, as the mode A has no cutoff frequency.

#200090 - $15.00 USD Received 25 Oct 2013; revised 29 Nov 2013; accepted 9 Dec 2013; published 20 Dec 2013
(C) 2013 OSA

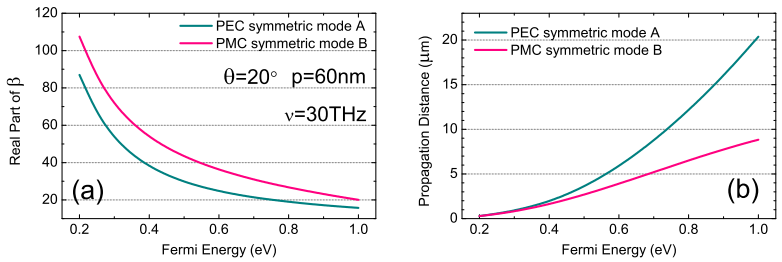

Fig. 5. The Fermi energy dependences of the momenta (**a**) and the propagation distances (**b**) for the PEC symmetric mode *A* and PMC symmetric mode *B*, with fixed plasmon frequency 30 THz. The geometric parameters of the waveguide keep the same with those in Fig. 3(a) and Fig. 4.

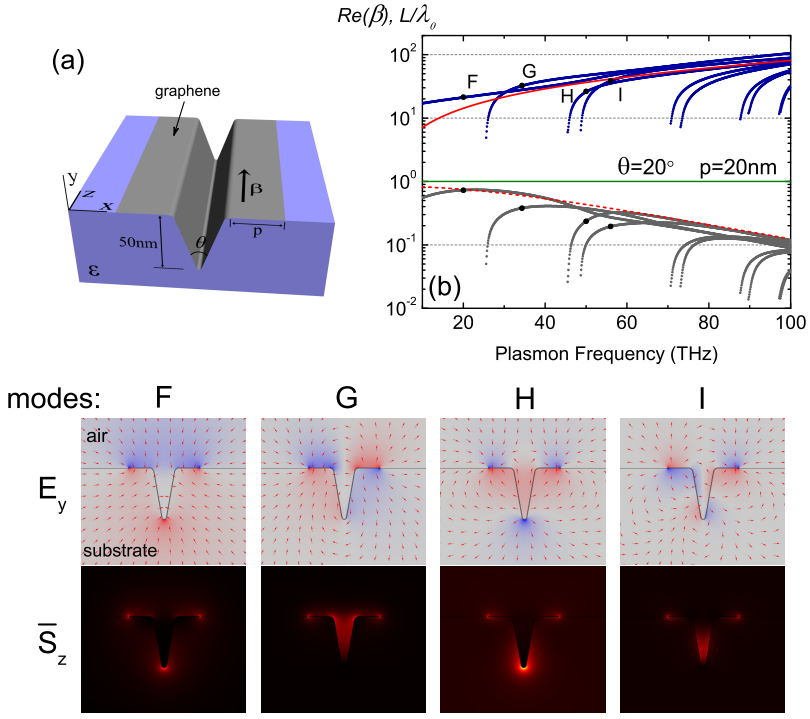

Fig. 6. Plasmon modes in the graphene groove waveguide. (**a**) The geometry of the groove waveguide. (**b**) The dispersion of the plasmon modes in the groove waveguide with $\theta = 20^\circ$ and $p = 20$ nm, the blue and gray lines are the normalized momenta and propagation distances respectively, the green line in the center corresponds to the momentum of light in vacuum. The lower eight plots show the E_y and time averaged S_z of the near-fields for the four modes labeled in (**b**), respectively.

#200090 - $15.00 USD Received 25 Oct 2013; revised 29 Nov 2013; accepted 9 Dec 2013; published 20 Dec 2013
(C) 2013 OSA

4. Surface plasmons in graphene groove waveguides

The graphene groove waveguides are almost identical to the wedge waveguides, the only difference is that high permittivity dielectric (substrate) is put on the other side of the graphene. The geometry of a groove waveguide is shown in Fig. 6(a), and the plasmon modes in a groove waveguide with the apex angle $\theta = 20^\circ$ and the brim width $p = 20$ nm are shown in Fig. 6(b). We find that the propagating plasmon modes supported by the graphene groove waveguide are very similar to the ones supported by the graphene wedge waveguide, and the corresponding modes have almost identical distributions of electric fields and energy fluxes (compare the lower panels in Fig. 1 and Fig. 6). Among the modes in the groove waveguide, modes F and H possess the PEC symmetry, modes G and I possess the PMC symmetry. However, the wave vectors of the plasmon modes in the groove waveguide are different from the ones in the wedge waveguide, which is due to the difference of permittivity. For the PMC symmetric modes G and I, the electromagnetic fields mainly stay in the air, in contrast to the graphene wedge modes B and C (see Fig. 1). As a result, momenta of the modes G and I are lower than the modes B and C at the same frequency. The same phenomenon also exists for the wedge mode D and the groove mode H, where the momentum of mode H is larger than the mode D.

5. Conclusions

In this paper, we have investigated the properties of surface plasmon modes in graphene wedge and groove waveguides using the finite element method. Our results show that graphene wedge waveguides can support propagating plasmons efficiently at terahertz-infrared waveband. These plasmon waveguide modes can be classified into two groups: the PEC and PMC symmetric modes. These two types of modes show different propagation characteristics, and the electromagnetic fields localize at different regions in the structures. More specifically, the PEC symmetric mode D, which catches our attention, achieves longer propagation distance than 2DGP at certain frequencies. The brim width and the Fermi energy dependence of the plasmon modes are also shown, which suggests that both the brim width of waveguides and Fermi energy of graphene can be used to tune the plasmon waveguide modes efficiently. The graphene groove waveguides support similar modes as the wedge waveguides, however, different regions where the electromagnetic fields concentrate lead to the differences of the wave vectors of the modes.

Acknowledgments

This work was supported by the National Basic Research Program of China (2013CB328702, 2010CB934101), the National Natural Science Foundation of China (11004112, 11374006, and 11304162), the 111 Project (B07013), International S&T Cooperation Program of China (2011DFA52870), Oversea Famous Teacher Project (MS2010NKDX0230). We also acknowledge the support from Institute of Scientific Computing of Nankai University.

#200090 - $15.00 USD Received 25 Oct 2013; revised 29 Nov 2013; accepted 9 Dec 2013; published 20 Dec 2013
(C) 2013 OSA